PREPARATION OF WOOD SAWDUST/Fe_2O_3 NANOCOMPOSITE AND ITS APPLICATION FOR ARSENIC (III) ION REMOVAL FROM AQUEOUS SOLUTIONS

HADI FALLAH MOAFI, REZA ANSARI and SAMIRA SADEGHNIA

Department of Chemistry, Faculty of Science, University of Guilan, Rasht, Iran
✉ *Corresponding author: Reza Ansari, ransari271@guilan.ac.ir*

Received March 19, 2017

This paper describes the potential use of α-Fe_2O_3 nanoparticles (α-Fe_2O_3 NPs) and α-Fe_2O_3 sawdust nanocomposite (α-Fe_2O_3/SD NC) toward the removal of arsenic from aqueous systems. The α-Fe_2O_3 NPs were synthesized by the co-precipitation method on sawdust. The samples were characterized using X-ray diffraction analysis (XRD) and scanning electron microscopy (SEM). SEM micrographs showed the formation of α-Fe_2O_3 NPs within 40-60 nm in size, which were homogeneously dispersed on the sawdust surface. The adsorption experiments were performed in a batch system. The optimum pH value for the maximum removal of As (III) was found at a value of about 7. The monolayer adsorption amounts calculated based on the Langmuir adsorption model were 83.33 and 58.80 mg g^{-1} for α-Fe_2O_3 and α-Fe_2O_3/SD, respectively. The kinetic data obeyed the pseudo-second-order kinetic model. The high adsorption capacity was attributed to the high surface area of α-Fe_2O_3 NPs and good dispersion α-Fe_2O_3 NPs on the sawdust substrate. The experimental results suggest that α-Fe_2O_3/SD NC is a promising and cost-effective adsorbent for the removal of As (III) ions from aqueous solutions.

Keywords: adsorption, α-Fe_2O_3 nanoparticles, α-Fe_2O_3/sawdust nanocomposite, As (III) removal

INTRODUCTION

Arsenic pollution in water sources has been reported all over the world due to its natural abundance in certain minerals. Arsenic compounds have been widely used in pesticides, insecticides, pigments, wood preservatives and in the manufacture of paper, glass and semiconductors that are used in integrated circuits.[1,2] The soluble inorganic species of arsenic in the environment include pentavalent arsenate (As^{5+}) and trivalent arsenite (As^{3+}). However, arsenite is more harmful than arsenate because of its higher attraction for protein, compared to arsenate, and is more mobile in the environment. Several methods have been developed for arsenic removal, including precipitation, adsorption, ion exchange, solvent extraction, nanofiltration, foam flotation and biological sequestration. Among them, adsorption technology is a good alternative method, which has been widely used due to its advantages, such as easier setup, ease of operation and handling, easier regeneration capacity or disposal of adsorbents and higher removal efficiency.[3,4] Various adsorbents, such as activated carbon, alumina, titania, zirconia, polystyrene-supported nano-Fe_3O_4, zeolite, kaolinite clay, cerium oxide, silica and iron oxides, have been employed for the removal of arsenic from water.[3-15] In recent years, iron based nanoscale particles have attracted great interest for water treatment and arsenic remediation.[5,7,16-19] An effective approach to increase the adsorptive capacity of iron oxide is to produce its nanosized particles. For example, J.G. Parsons *et al.*[16] synthesized Fe_3O_4, Mn_3O_4 and $MnFe_2O_4$ nanoadsorbents for sequestering arsenic from aqueous solutions. S. Luther *et al.*[5] utilized nanophase Fe_3O_4 and Fe_2O_3 for the removal of either As (III) or As (V) from aqueous solutions. Another case, S. Lin *et al.*[19] used magnetic γ-Fe_2O_3 NPs synthesized by the co-precipitation method to remove As (III) and As (V) ions from aqueous solutions.

A number of publications have reviewed the coating of iron oxide on different substances for removal of arsenic.[7,20-25] For example; T.V. Nguyen *et al.*[20] reported the arsenic removal by an iron oxide coated sponge. They found that maximum adsorption capacity of the iron oxide coated sponge for As (III) and As (V), calculated by the Sips isotherm, was 4.2 and 4.6 mg g^{-1} of iron oxide coated sponge, respectively. S.K. Maji *et al.*[21] have used iron-oxide-coated natural rock as an adsorbent for arsenic removal. Their results showed that maximum adsorptive capacity of the iron-oxide-coated natural rock was 0.36 mg g^{-1}. W. Jiang *et al.*[7] also utilized spherical polystyrene-supported nano-

Fe_3O_4 for arsenate removal from water. They prepared the nano-Fe_3O_4 coated onto the outer surface of polystyrene (PS) beads of 350-400 nm in diameter by the hetero-coacervation method. They found that the maximum adsorption capacity of PS-Fe_3O_4 was 139.3 mg g^{-1}, which is 77.7% greater than that of bulky Fe_3O_4. A. Gupta *et al*.[26] recently reported chitosan and iron−chitosan-coated sand filters for the removal of both As (III) and As (V) from aqueous systems. They optimized various parameters including pH, equilibration time, initial arsenic concentration and adsorbent dosage for maximum adsorption. They found that the Langmuir monolayer adsorption capacity was found to be 17 and 23 mg g^{-1} for chitosan-coated sand and 26 and 56 mg g^{-1} for iron−chitosan-coated sand at pH 7 for As (III) and As (V), respectively.

Today, alternative adsorbents derived from renewable resources or less expensive natural materials have attracted much interest for the removal of pollutants from wastewaters. Sawdust is a waste material that is one of the most attractive biomaterials used for removing heavy metals and organic pollutants from aqueous media. The capability of treated and untreated sawdust to remove pollutants from aqueous solutions has been studied.[27-31] The objective of this study was to develop an iron oxide/sawdust composite for effective removal of As (III) ions from aqueous wastes. The iron oxide nanomaterials were synthesized using the precipitation method. The adsorption experiments were performed in a batch system. Batch studies were performed to determine the capacities of α-Fe_2O_3 NPs and α-Fe_2O_3/SD NC for As (III) removal. In order to find out the optimized adsorption conditions for maximum removal, as well as driving kinetics and isotherm data, the effect of some important parameters, such as pH, adsorbent dose, initial concentration and contact time, were studied.

EXPRIMENTAL

Materials

Ferric chloride ($FeCl_3$), ammonia (NH_3, 33%) and arsenic trioxide (As_2O_3) were of analytical grade and purchased from Merck chemical company (Germany). All the solutions were prepared using deionized water. As_2O_3 was dissolved in deionized water as a stock solution of As (III) (10 mM) for further use. The sawdust was obtained from a local carpentry working with Narra wood. The sawdust was washed several times with deionized water to remove any surface impurities and dried at 80 °C for 24 h. The sawdust was ground and sieved before preparation of Fe_2O_3/SD NC.

Preparation of α-Fe_2O_3 nanoparticles and α-Fe_2O_3/sawdust nanocomposite

The typical procedure for the synthesis of α-Fe_2O_3 NPs is based on the method described in the literature with minor changes detailed in another study.[5] In a typical procedure, 0.50 L metal ion solutions of 0.50 M Fe (III) (from $FeCl_3$) were prepared. Iron (III) hydroxide nanoparticles were prepared by adding of 1.0 M NH_3 solution for approximately 2 h until the pH of the solution reached 9.0. After the precipitation reaction was completed, the solution was heated to a temperature of 100 °C for 1 h. The solutions were then left to cool, the nanoparticles were collected using the vacuum filtration technique and finally rinsed three times with deionized water to remove any possible by-products or impurities. The separated Fe_2O_3 NPs were then dried at 100 °C in an oven for several hours until they reached a constant weight and stored before use for As (III) removal. For preparation of α-Fe_2O_3/SD NC, the same procedure was used. For preparation, 5.0 g sawdust (35-50 mesh) was added to 0.50 L of 0.50 M $FeCl_3$ solution and stirred for two hours at room temperature. Afterwards, NH_3 solution (1.0 M) was slowly added into the mixture of metal ion-sawdust for 2 h under vigorous stirring and then the mixture was heated at 100 °C for another 2 h. Subsequently, the α-Fe_2O_3/SD particles were rinsed with sufficient deionized water and dried for several hours in an oven at 100 °C.

Point of zero charge

The point of zero charge (pHpzc) of the α-Fe_2O_3 NPs and α-Fe_2O_3/SD NC was determined based on the method described in the literature.[32] For this purpose, 45 mL of KNO_3 solution of known concentration was transferred to a series of 100 mL Erlenmeyer flasks. The pH_i values of the solution were approximately adjusted from 3.0 to 11 by adding either 0.1N HNO_3 or NaOH. The total volume of the solution in each flask was adjusted to exactly 50 mL by adding KNO_3 solution of the same concentration. The pH_i of the solutions was then accurately recorded. Then, 0.10 g of α-Fe_2O_3 nanoparticles were added to each flask. The suspensions were then manually shaken and allowed to equilibrate for 48 h with intermittent shaking. The final pH values of the supernatant liquid (pH_f) were recorded. The difference between the initial and final pH (ΔpH) values ($\Delta pH = pH_f - pH_i$) was plotted against the pH_i. The point of intersection of the resulting curve at which ΔpH = 0 gave the pHpzc.[32] The above procedure was repeated for the determination of pHpzc of Fe_2O_3/SD NC.

Analysis and characterization techniques

The X-ray powder diffraction patterns were collected using a Philips (PW-1840) XRD system with Ni-filtered Cu Kα (λ = 1.5418 A^o) radiation at 40 kV and 30 mA. The 2θ range used in the measurement was from 10^o to 70^o. To investigate the morphology of the samples, scanning electron microscopy (SEM) images were obtained on a Philips XL30. A digital coulometer (model ZCM 761, Iran) was used for coulometric determination of As (III). A digital desktop pH meter (Metrohm 827) was employed for pH control.

Batch experimental procedures

All adsorption equilibrium experiments were conducted in a batch system. Adsorption studies were carried out by shaking 0.20 g of the adsorbent with 50 mL of the aqueous solutions of As (III) ions with an initial concentration of 2 mM in a conical flask at room temperature under stirring 200 rpm. The mixtures were filtered out and analyzed for As (III) ions concentrations. All the As (III) solutions required for the experiments were freshly prepared by diluting the stock solution. The analysis of As (III) was carried out using coulometeric titration.[33] The end point was detected potentiometrically with high precision, employing Pt and Ag/AgCl in 3M KCl as indicator and reference electrodes, respectively. All As (III) solutions were used at neutral pH and the procedure was performed at room temperature. The effect of pH on the equilibrium uptake of As (III) ion was determined. The pH of the As (III) solution was adjusted by using either HCl or NaOH solutions, and was varied within the range of 3-11. All the results reported in this paper are the average of at least triplicate measurements and the maximum expected error was of about ±5%. After 1 h of agitation, the adsorbent was separated from the test solutions by filtration and the filtrates were analyzed for residual As (III). The adsorption experiments were also conducted to determine the optimum pH, the equilibrium time and dosage of the α-Fe_2O_3 NPs and α-Fe_2O_3/SD NC for maximum adsorption. At optimum pH, the effect of the adsorbent dose on the removal of As (III) was studied using 50 mL of 2.0 mM solution at 25 °C. The mass of the adsorbents was varied from 0.05 g to 0.5 g. The efficiency of As (III) removal was determined using Eq. (1):

$$\text{Percent adsorption (\%)} = (C_0 - C_e/C_0) \times 100 \quad (1)$$

where C_0 and C_e are the initial and equilibrium concentrations (mg L^{-1}) of As (III), respectively.

The adsorption capacities (q_t, mg g^{-1}) of α-Fe_2O_3 NPs and α-Fe_2O_3/SD NC were also calculated using Eq. (2):[34-36]

$$q_t = (C_0\text{-}C_t)V/W \quad (2)$$

where C_0 (mg L^{-1}) and C_t (mg L^{-1}) are the concentration of arsenic initially and at time t (min), V (L) is the volume of the sample solution, and W (g) is the weight of the adsorbent.

The equilibrium sorption capacity (q_e) of the adsorbent was also calculated using Eq. (3):

$$q_e = (C_0 - C_e)V/W \quad (3)$$

where W is the adsorbent mass (g) and V is the volume of solution (L).

RESULTS AND DISCUSSION

X-ray diffraction analysis (XRD)

The XRD patterns of initial sawdust, α-Fe_2O_3 coated sawdust and pure α-Fe_2O_3 NPs are exhibited in Figure 1. In the XRD pattern of sawdust (Fig. 1a), the bulk of the X-ray signal originated from the sawdust substrate. Figure 1(b) shows the XRD pattern of α-Fe_2O_3 covered sawdust. Since the amount of α-Fe_2O_3 was not high on the sawdust surface, the α-Fe_2O_3 NPs on the fiber surface did not show good crystalline phase intensity. The XRD pattern for the α-Fe_2O_3 NPs (Fig. 1c) reveals the following planes: 104, 110, 113, 024, 116, 214 and 300, which correspond to the diffraction planes in α-Fe_2O_3.[37] No peaks of any other phases or impurities were detected in the XRD patterns of α-Fe_2O_3 NPs, demonstrating the high purity of the α-Fe_2O_3 NPs.

Morphology study

In order to investigate the morphology of the obtained samples, the α-Fe_2O_3 NPs, as well as the untreated and treated sawdust after coating with α-Fe_2O_3 NPs, were studied by SEM (Fig. 2). Figure 2a and 2b show the surface of the pristine sawdust. The SEM micrograph exhibits the rough and porous surface of the sawdust. A comparison between the SEM images of the treated and untreated sawdust clearly shows that treated sawdust is covered by continuous and dispersed α-Fe_2O_3 NPs. SEM analysis of the α-Fe_2O_3 deposited onto sawdust indicates that the particle size of the deposited hematite on the sawdust surface is less than 100 nm (Fig. 2c and 2d). The SEM micrographs clearly show the formation of α-Fe_2O_3 NPs within 40-60 nm in size, which have been homogeneously dispersed on the sawdust surface. As the SEM images of the α-Fe_2O_3 NPs indicate (Fig. 2e and 2f), the

morphology of the α-Fe_2O_3 NPs is similar to that of the nanoparticles coated on the sawdust surface, but the α-Fe_2O_3 NP powder displays more agglomerates than the nanocomposite (α-Fe_2O_3/SD NC).

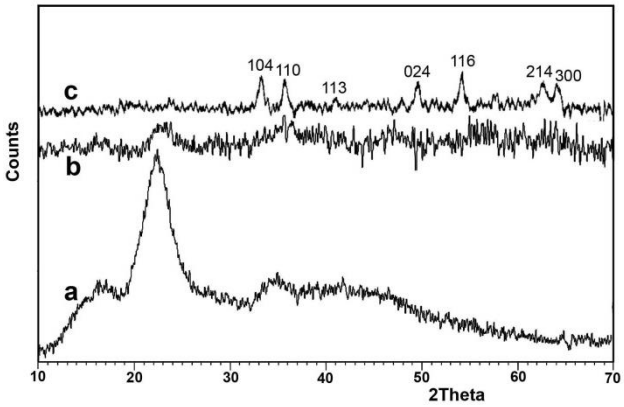

Figure 1: XRD patterns of: (a) initial sawdust, (b) α-Fe_2O_3 coated sawdust and (c) pure α-Fe_2O_3 NPs

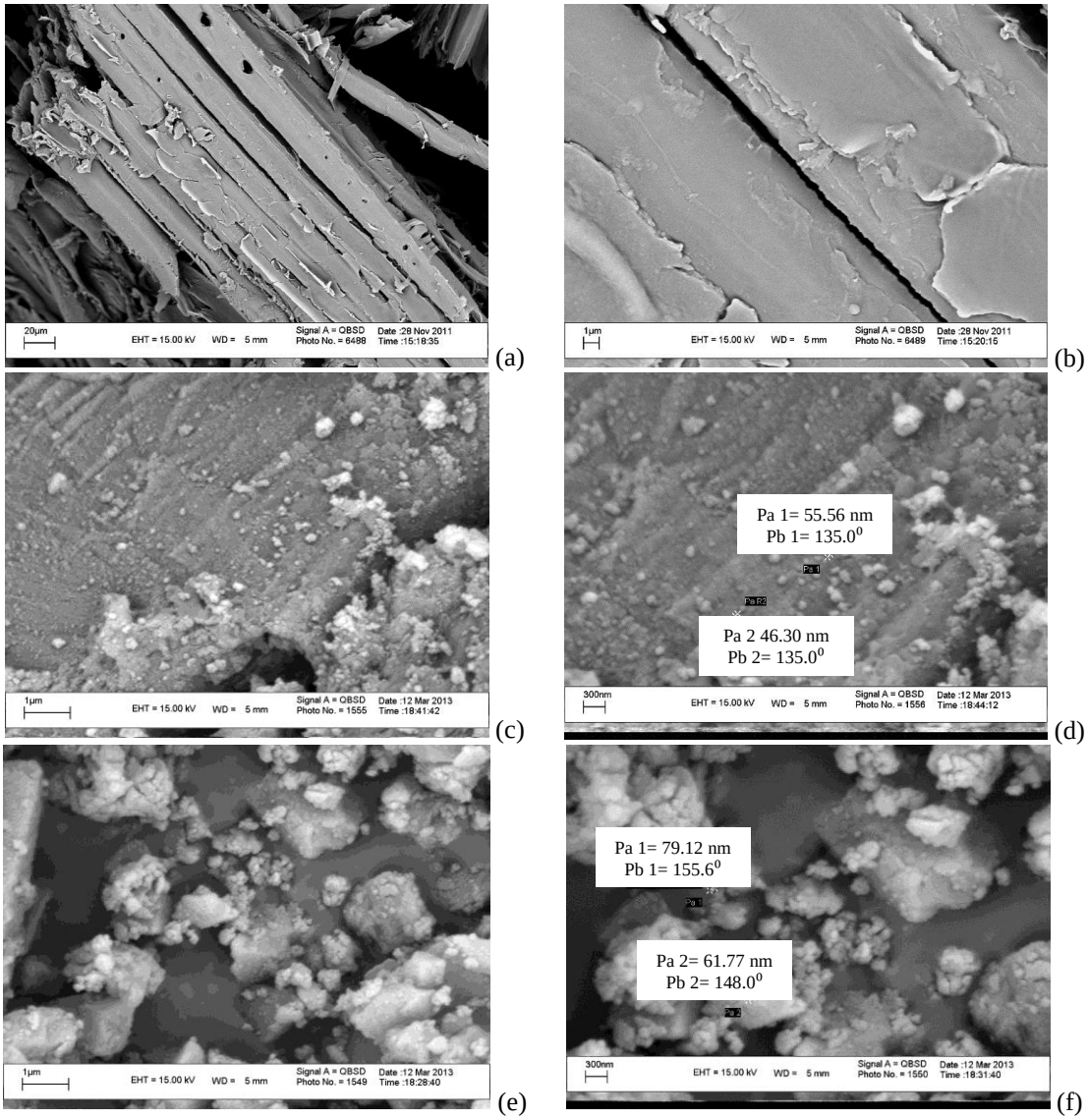

Figure 2: SEM images of: (a, b) sawdust, (c, d) α-Fe_2O_3 coated sawdust and (e, f) α-Fe_2O_3 NPs

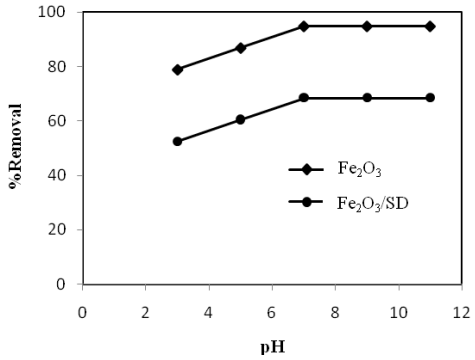

Figure 3: Effect of pH on the As (III) adsorption on α-Fe_2O_3 NPs and α-Fe_2O_3/SD NC

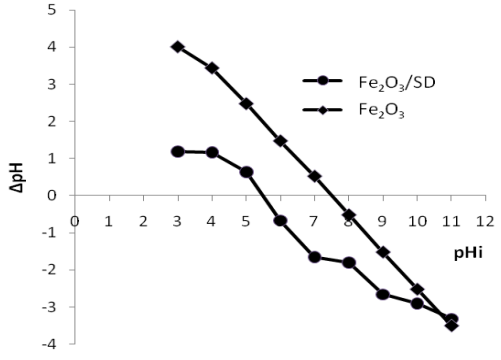

Figure 4: Point of zero charge of α-Fe_2O_3 NPs and α-Fe_2O_3/SD NC

Optimization of adsorption conditions

Effect of initial solution pH

The pH is one of the most important environmental factors that strongly influence the adsorption of heavy metals.[31] In order to determine the optimum pH for maximum removal of arsenic on α-Fe_2O_3 NPs and α-Fe_2O_3/SD NC, the equilibrium sorption of arsenic was studied over a pH range of 3-11. Considering the poor adsorption of As (III) onto untreated sawdust (<5%), compared to that onto Fe_2O_3/SD NC, under the same conditions, the adsorption data for SD are not shown. As indicated in Figure 3, the uptake of As (III) ion depends on pH, it increases with the increase in pH from 3.0 to 7.0 for both Fe_2O_3 NPs and α-Fe_2O_3/SD NC. Maximum As (III) removal was observed at a pH value of about 7. As a result, the optimum pH for As (III) adsorption was established as 7.0 and the other adsorption experiments were performed at this pH value. As indicated, above this pH range, the uptake of As (III) ion does not change. This can be explained as follows: at a pH value between 5-7, As (III) exists mostly as $As(OH)_3$.[38] So, the increase in As (III) removal at this pH can be due to the strong interactions, such as H-bonding between $As(OH)_3$ species and the hydroxyl groups on the surface of the adsorbent due to iron oxide nanoparticles. Because of the poor adsorption of As (III) onto untreated sawdust, further experiments were carried out for only Fe_2O_3 NPs and α-Fe_2O_3/SD NC.

Determination of pH_{PZC} of the adsorbent

Determination of the point of zero charge of the adsorbents is important in elucidating the adsorption mechanism. The adsorption of cations is favored at pH > pH_{PZC}, while anion adsorption is favored at pH < pH_{PZC}. The specific adsorption of cations shifts pH_{PZC} towards lower values, whereas the specific adsorption of anions shifts pH_{PZC} towards higher values.[32,39] Figure 4 presents the point of zero charge of α-Fe_2O_3 NPs and α-Fe_2O_3/SD NC. Tthe plot of the evolution of solution pH (ΔpH) *versus* initial pH (pH_i) shows that with increasing initial solution pH, the pH change became more negative and the zero value of ΔpH was reached at pH_i values of 7.5 and 5.5, which are considered as the pH_{PZC} of α-Fe_2O_3 NPs and α-Fe_2O_3/SD NC, respectively.

Effect of contact time

The effect of contact time on the adsorption of As (III) ions was studied by shaking the mixture of 0.20 g adsorbent (α-Fe_2O_3 NPs and α-Fe_2O_3/SD NC) with 50 mL of aqueous solutions of As (III) ions with an initial concentration of 2.0 mM at neutral pH value. The time dependence of As (III) adsorption is presented in Figure 5. The data obtained from the adsorption of As (III) ion on the α-Fe_2O_3 NPs and α-Fe_2O_3/SD NC indicate that the adsorption increases with an increasing contact time. The plot reveals that the rate of percentage removal of As (III) ion is initially high, which is probably due to the availability of a larger surface area of the α-Fe_2O_3 NPs and α-Fe_2O_3/SD NC for the adsorption of arsenic ions. The maximum percentage removal of As (III) ion was attained after 60 min of stirring time. The adsorption did not changed much with further increase in contact time. Therefore, the contact time of 60 min was sufficient to achieve equilibrium for As (III) adsorption. Consequently, in further experiments, the shaking time was set to 60 min. Figure 5 shows that the percentage adsorption of As (III) ions onto α-Fe_2O_3 NPs is higher than onto α-Fe_2O_3/SD NC, and the adsorption of As (III) ions onto α-Fe_2O_3 NPs was less time dependent, compared to that onto α-Fe_2O_3/SD NC.

Effect of adsorbent dosage

Adsorbent dosage is an important parameter as it determines the capacity of an adsorbent for adsorption of an adsorbate. In these experiments, various amounts of α-Fe_2O_3 NPs and α-Fe_2O_3/SD NC (from 0.050 to 0.50 g) were used for adsorption of an As (III) solution (50 mL, 2.0 mM) at room temperature. Figure 6 shows the effect of adsorbent dosage on the removal efficiency (% removal) of As (III) from the aqueous solution. The results show that the adsorption increases with the increase in the dose of α-Fe_2O_3 NPs and α-Fe_2O_3/SD NC. In the case of α-Fe_2O_3 NPs, it is observed that the removal efficiency increases from 36.8% to 94.7% with an increase in adsorbent dose from 0.05 g to 0.20 g. For α-Fe_2O_3/SD NC, the increase in the adsorbent dosage from 0.050 to 0.30 g resulted in an increase of adsorption from 26.3% to 81.3.7%. This is due to the increase in the surface area and the availability of more active sites of the adsorbent for uptake of As (III) ions. The lower sorption capacity found for α-Fe_2O_3/SD NC, compared to α-Fe_2O_3 NPs, under the same dosages, is also clearly due to the lower percentage of α-Fe_2O_3 in the composite. Beyond the optimum dosage, the removal efficiency remains unchanged with further increases in the adsorbent dosage (>0.20 g for α-Fe_2O_3 NPs and α-Fe_2O_3/SD NC). This seems to be due to the binding of almost all the ions to the adsorbent and the establishment of equilibrium.[34] It has been reported that there are many factors that can contribute to effect of adsorbent dosage on the efficiency of adsorption.[34,40] The most important factor is that the adsorption sites remain unsaturated during the adsorption process. As the adsorbent dosage is increased, the adsorption increases slightly, resulting from the lower adsorptive capacity utilization of the adsorbent. Another reason may be the aggregation/agglomeration of adsorbent particles at higher dosages, which would lead to a decrease in the surface area and an increase in the diffusion path length. The particle interaction at higher adsorbent dosage may also help desorb some of the loosely bound metal ions from the sorbent surface.[40]

Effect of initial concentration

The initial metal ion concentration is another important variable that can affect the adsorption process. The rate of adsorption or adsorption capacity is a function of initial metal ion concentration. The effect of arsenic concentration on the adsorption was studied under optimized pH. For this investigation, 50 mL of As (III) ion solution, with different initial concentrations, was used for adsorption onto 0.20 g of Fe_2O_3 NPs and α-Fe_2O_3/SD NC. The concentrations of As (III) varied from 1.0 to 10.0 mM. The effect of the initial As (III) concentration on the removal efficiency of the selected adsorbents is shown in Figure 7. As the results indicate, both Fe_2O_3 NPs and α-Fe_2O_3/SD NC are more efficient adsorbents at low concentrations of arsenic ions. The decrease in adsorption percentage at higher concentrations might be caused by the relatively smaller numbers of active sites available at higher arsenic concentrations.

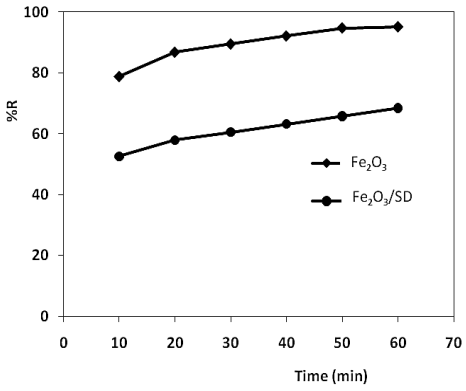

Figure 5: Effect of contact time on As (III) adsorption onto α-Fe_2O_3 NPs and α-Fe_2O_3/SD NC

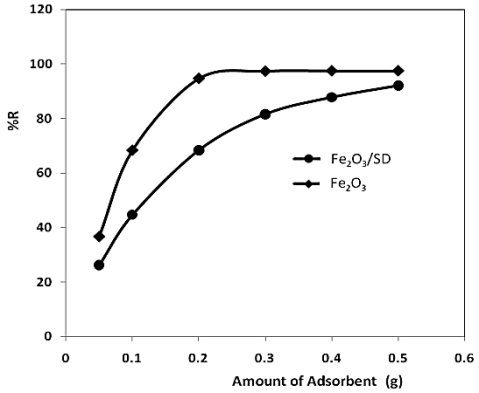

Figure 6: Effect of adsorbent dosage of α-Fe_2O_3 NPs and α-Fe_2O_3/SD NC in the removal of As (III)

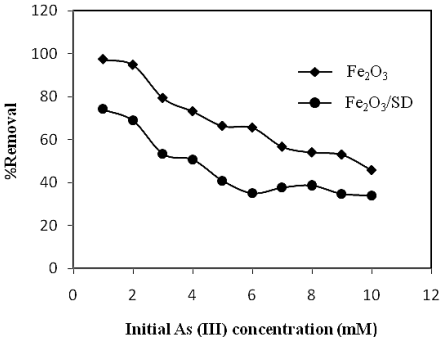

Figure 7: Effect of initial concentration of As (III) on adsorption

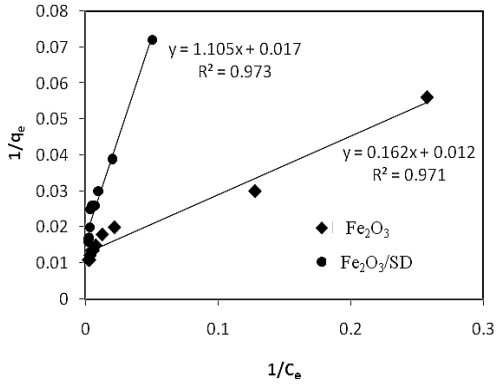

Figure 8: Langmuir isotherm plot of adsorption equilibrium data (conditions: 298 K, adsorbent dose 0.20 g, contact time 60 min, pH 7.0)

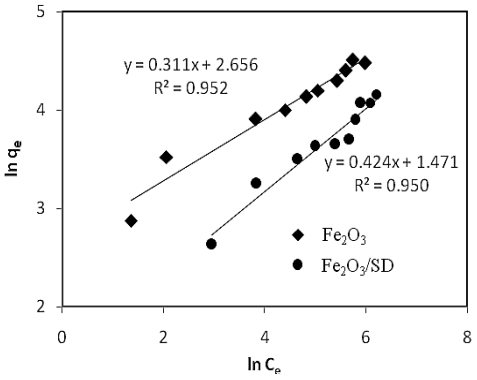

Figure 9: Freundlich isotherm plot of adsorption equilibrium data (conditions: 298 K, adsorbent dose 0.20 g, contact time 60 min, pH 7.0)

Adsorption isotherms

The distribution of the adsorbate between the liquid phase and the solid adsorbent is a measure of the equilibrium in an adsorption process and can be investigated through various models. In this study, two popular adsorption isotherms suggested by Langmuir and Freundlich were employed for analysis of the adsorption data.[41] The Langmuir isotherm is based on three assumptions, namely (i) adsorption cannot proceed beyond monolayer coverage, (ii) all surface sites are equivalent, and (iii) the ability of a molecule to adsorb at a given site is independent of the occupation of neighboring sites.[3] The Freundlich model assumes physicochemical adsorption on heterogeneous surfaces. The obtained data were analyzed according to the linearized forms of the Langmuir and Freundlich isotherms,[42,43] using Eqs. (4) and (5):

$$\text{Langmuir } 1/q_e = 1/q_m.b.C_e + 1/q_m \quad (4)$$

$$\text{Freundlich } \ln q_e = \ln k_F + 1/n\ (\ln C_e) \quad (5)$$

where q_e is the amount of adsorbed As (III) per unit mass of adsorbent at equilibrium (mg g^{-1}), C_e is equilibrium concentration of As (III) in the solution (mg L^{-1}), q_m is the maximum monolayer adsorption capacity (mg g^{-1}), b, K_F and n are the Langmuir and Freundlich adsorption coefficients, respectively.

For this investigation, 0.20 g of the adsorbents were used for the adsorption of 50 mL of an As (III) solution with different initial concentrations (1 to 10 mM). The experiments were conducted at room temperature for 60 min (pH = 7). The solutions were analysed for the remaining arsenic concentrations (C_e) and then the adsorption isotherms were derived using Eq. (3) (Figs. 8 and 9). From the linear plots of the obtained isotherms, the parameters of K_F, b, n and q_m were determined and are summarized in Table 1. It is noted that the adsorption capacity of SD toward As (III) under the studied concentration ranges was negligible and approached zero. The α-Fe_2O_3 NPs exhibited much higher adsorption capacity toward As (III) than the α-Fe_2O_3/SD NC. The monolayer adsorption capacity (q_m) was obtained as 83.33 and 58.8 mg g^{-1} for α-$Fe_2O_3$and α-Fe_2O_3/SD NC, respectively. The adsorption of As (III) onto α-Fe_2O_3 NPs and α-Fe_2O_3/SD NC follows both the Freundlich and the Langmuir models. Based on the higher values of the correlation coefficients (R^2) for the Langmuir model, compared to

the Freundlich model, the adsorption data seem to be described by the Langmuir model more favorably. On the other hands, the Langmuir model is more suitable than the Freundlich model for describing the adsorption process, indicating that the adsorption of As (III) on α-Fe_2O_3 NPs and α-Fe_2O_3/SD NC is homogenous.

The favorability of the adsorption process was also represented in terms of the dimensionless separation factor R_L, which is defined by Eq. (6):[36]

$$R_L=1/(1+bC_0) \quad (6)$$

where C_0 is the initial concentration (mg L^{-1}) and b is the Langmuir constant (L mg^{-1}). The value of R_L indicates that the adsorption process is unfavorable when $R_L > 1$, linear when $R_L = 1$, favorable when $R_L < 1$ and irreversible when $R_L = 0$. For all the studied cases, the R_L values fall between 0 and 1 (Table 1), confirming the favorable nature of the adsorption of As (III) onto α-Fe_2O_3 and α-Fe_2O_3/SD.

A comparison of the maximum capacities (q_m) of α-Fe_2O_3 NPs and α-Fe_2O_3/SD NC with some other adsorbents reported in the literature are given in Table 2. The adsorption capacities of α-Fe_2O_3 NPs and α-Fe_2O_3/SD NC were relatively high when compared with other adsorbents reported previously. Differences of metal ion uptake are due to the properties of each adsorbent, such as structure, functional groups and surface area.[34]

Table 1
Langmuir and Freundlich isotherm constants for As (III) adsorption onto α-Fe_2O_3 nanoparticles and α-Fe_2O_3/SD nanocomposite

Adsorbent	Langmuir model				Freundlich model		
	q_m (mg g^{-1})	b (L mg^{-1})	R_L	R^2	K_F (mg g^{-1})(mg L^{-1})$^{-1/n}$	n	R^2
α-Fe_2O_3 NPs	83.33	0.074	0.018	0.9711	14.24	3.21	0.9528
α-Fe_2O_3/SD NC	58.80	0.0154	0.079	0.9731	4.35	2.36	0.9505

Table 2
Comparison of adsorption capacity of α-Fe_2O_3 and α-Fe_2O_3/SD nanocomposite with other adsorbents for As (III) removal

Adsorbent	Conditions (contact time, temperature, pH)	q_m (mg g^{-1})	Reference
α-Fe_2O_3 NPs	1 h, 25 ^oC, pH 7	83.33	This study
γ-Fe_2O_3	3 h, 30 ^oC, pH 6	59.20-74.80	[19]
Fe_3O_4	24 h, 25 ^oC, pH 6	78.40	[7]
Fe_3O_4, α-Fe_2O_3	1 h, 25 ^oC, pH 6	8.20, 1.25	[5]
Fe_3O_4, α-Fe_2O_3	24 h, 25 ^oC, pH 6	5.68, 20.00	[5]
Mixed magnetite and maghemite nanoparticles	24 h, 25 ^oC, pH 2	3.69	[41]
α-Fe_2O_3/SD NC	1 h, 25 ^oC, pH 7	58.8	This study
Ascorbic acid coated Fe_3O_4 nanoparticle	0.5 h, 25 ^oC, pH 7	46.06	[17]
Iron oxide-coated natural rock	2 h, 25 ^oC, pH 7.5	0.029	[24]
Iron oxide coated cement	2 h, 25 ^oC, pH 7	0.69	[25]
Iron oxide coated sponge	Sips isotherm	4.2	[20]

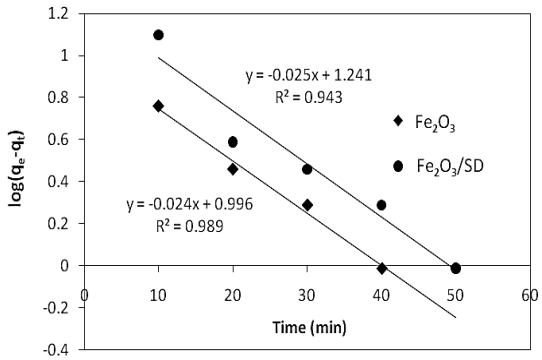

Figure 10: Pseudo-first order plot for As (III) adsorption onto Fe_2O_3 NPs and α-Fe_2O_3/SD NC

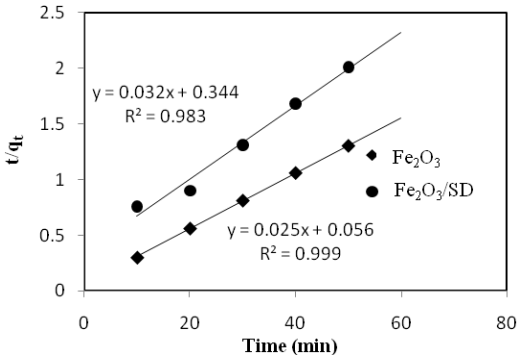

Figure 11: Pseudo-second order plot for As (III) adsorption onto Fe_2O_3 NPs and α-Fe_2O_3/SD NC

Adsorption kinetics

In order to investigate the kinetic mechanism of As (III) sorption onto the α-Fe_2O_3 NPs and α-Fe_2O_3/SD NC, several kinetic models, including the pseudo-first-order (Eq. (7)), pseudo-second-order (Eq. (8)) and intraparticle diffusion model (Eq. (9)), were examined.[44-46] Adsorption kinetic experiments were conducted with an adsorbent dose of 0.20 g at 25 ºC at an initial arsenic concentration of 2.0 mM.

$$\log (q_e - q_t) = \log q_e - k_1 t / 2.303 \quad (7)$$

$$t / q_t = 1 / k_2 q_e^2 + t / q_e \quad (8)$$

where q_e (mg g^{-1}) and q_t (mg g^{-1}) are the amounts of As (III) ions adsorbed at equilibrium and at time t (min), respectively, k_1 (min^{-1}) and k_2 (g min^{-1} mg^{-1}) are the pseudo-first-order and pseudo-second-order adsorption rate constant, respectively.

The values of k_1 and q_e for the pseudo-first-order model were determined from the slope and intercept of the plot of $\log(q_e-q_t)$ against t (Fig. 10). The values of k_2 and q_e for the pseudo-second-order model were calculated from the slope ($1/q_e$) and intercept ($1/K_2q_e^2$) of the linear plot of t/q_t *versus* t (Fig. 11). The resulting kinetics data are summarized in Table 3. The applicability of the kinetic models for describing the adsorption process was evaluated by the values of the correlation coefficients (R^2). It can be seen that the values of the correlation coefficients for the pseudo-second-order model are greater than those of the pseudo-first-order model. Moreover, the calculated values of q_e for the pseudo-second-order model are closer to the experimental values of q_e (Table 3). Therefore, it could be concluded that the sorption of As (III) onto α-Fe_2O_3 NPs and α-Fe_2O_3/SD NC follows the pseudo-second-order kinetic model.

The intraparticle diffusion model was also explored to analyze the nature of the rate-controlling step in adsorption. The model is represented by the following Weber–Morris equation:[46]

$$q_t = k_{ip} t^{0.5} + C \quad (9)$$

where k_{ip} is the intraparticle diffusion rate constant (mg g^{-1} $min^{-1/2}$) and C is the intercept related to the thickness of the boundary layer.[32,36]

The plots of qt *versus* $t^{1/2}$ are shown in Figure 12. According to this model, if intraparticle diffusion is the sole rate-controlling step in the adsorption process, the plot of q_t *versus* $t^{1/2}$ should be linear and should go through the origin with a slope k_{id} and intercept *C*.[22,32] As the results show (Fig. 12), the plot of qt *versus* $t^{1/2}$ is not linear over the entire time period and the straight lines do not pass through the origin, indicating that intraparticle diffusion is not the rate-limiting step. This implies that more than one process is involved in controlling the adsorption of As (III) ions onto the selected adsorbents.

Table 3
Kinetic parameters for As (III) adsorption onto α-Fe_2O_3 nanoparticles and α-Fe_2O_3/SD nanocomposite

Adsorbent	Pseudo-first order			Pseudo-second order				Intraparticle diffusion		
	$q_{e,cal}$ (mg g^{-1})	K_1 (min^{-1})	R^2	$q_{e.exp}$ (mg g^{-1})	$q_{e,cal}$ (mg g^{-1})	K_2 (g mg^{-1} min^{-1})	R^2	K_{id} (mg $g^{-1}min^{-1/2}$)	C (mg g^{-1})	R^2
α-Fe_2O_3 NPs	9.91	0.055	0.989	38.78	40	0.01	0.999	1.43	28.88	0.968
α-Fe_2O_3/SD NC	17.42	0.06	0.943	25.8	31.25	0.003	0.983	2.15	9.56	0.774

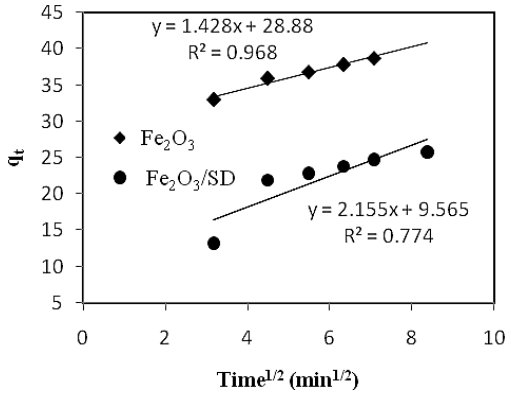

Figure 12: Intraparticle diffusion model plot for As (III) adsorption onto Fe_2O_3 NPs and α-Fe_2O_3/SD NC

CONCLUSION

In this study, an α-Fe_2O_3/SD nanocomposite was prepared by the co-precipitation method and applied as adsorbent for the elimination of As (III) from aqueous solutions. The performance of the prepared samples in removing arsenic from an aqueous solution was investigated by batch adsorption experiments. While sawdust itself is a poor adsorbent for As (III) ions, the α-Fe_2O_3/SD NC proved its efficiency. The optimum pH for the maximum removal of As (III) by α-Fe_2O_3 NPs and α-Fe_2O_3/SD NC was found to be about 7.0. The adsorption and equilibrium data closely follow the Langmuir adsorption isotherm, demonstrating that the monolayer adsorption mechanism and chemisorption process occur. The monolayer adsorption capacity (q_m), as estimated from the Langmuir isotherm, is 83.33 and 58.8 mg g^{-1} for α-Fe_2O_3 NPs and α-Fe_2O_3/SD NC, respectively, which is much higher than that reported for many other adsorbents studied. The kinetic data and the correlation coefficients (R^2) confirm that the sorption of As (III) onto α-Fe_2O_3 NPs and α-Fe_2O_3/SD NC follows the pseudo-second-order kinetic model. The high adsorption capacity, easy and cost-effective synthesis of the α-Fe_2O_3 NPs and α-Fe_2O_3/SD NC further suggest its potential application for removal of toxic metal ions such as As (III) in industrial wastewater treatment.

ACKNOWLEDGMENT: The authors are highly thankful to the University of Guilan for providing financial assistance for this research project.

REFERENCES

1 A. Benhamou, J. P. Basly, M. Baudu, Z. Derriche and R. Hamacha, *J. Colloid Interface Sci*., **404**, 135 (2013).
2 S. H. Dong, K. S. Jin, B. Bill and A. W. Ahmed, *J. Colloid Interface Sci*., **392**, 311 (2013).
3 S. Suparna and S. Priyabrata, *J. Hazard. Mater*., **227-228**, 68 (2012).
4 S. H. Dong, A. W. Ahmed and B. Bill, *J. Colloid Interface Sci*., **348**, 591 (2010).
5 S. Luther, N. Borgfeld, J. Kim and J. G. Parsons, *Microchem. J*., **101**, 30 (2012).
6 K. Hristovski, A. Baumgardner and P. Westerhoff, *J. Hazard. Mater*., **147**, 265 (2007).
7 J. Wei, C. Xubin, N. Yingjie and P. Bingcai, *J. Hazard. Mater*., **243**, 319 (2012).
8 L. Zhaohui, B. Ryan, M. Zoe and H. Hong, *Micropor. Mesopor. Mater*., **105**, 291 (2007).
9 A. Saada, D. Breeze, C. Crouzet, S. Cornu and P. Baranger, *Chemosphere*, **51**, 757 (2003).
10 L. Ronghui, L. Qi, G. Shian and K. S. Jian, *Chem. Eng. J*., **185–186**, 127 (2012).
11 G. Kaushik, B. Sayan, C. Dhrubajyoti, M. Aniruddha, B. Harishankar *et al*., *Chem. Eng. J*., **172**, 219 (2011).
12 C. Qigang, L. Wei and Y. Wei-Chi, *J. Hazard. Mater*., **184**, 515 (2010).
13 R. Sandoval, A. M. Cooper, K. Aymar, A. Jain and K. Hristovski, *J. Hazard. Mater*., **193**, 296 (2011).
14 F. Hong-Tao, S. Ting, X. Hong-Bo, Y. Yan-Jie, T. Qi *et al*., *Desalination*, **278**, 238 (2011).
15 Y.-M. Zheng, L. Yu, D. Wu and J. P. Chen, *Chem. Eng. J*., **188**, 15 (2012).
16 J. G. Parsons, M. L. Lopez, J. R. Peralta-Videa and J. L. Gardea-Torresdey, *Microchem. J*., **91**, 100 (2009).
17 F. Liyun, C. Minhua, M. Xiaoyu, Z. Yongshuang and H. Changwen, *J. Hazard. Mater*., **217**, 439 (2012).
18 W. Kun, L. Rui-Ping, L. Hui-Juan, L. Hua-Chun and Q. J. Jiu-Hui, *J. Hazard. Mater*., **239–240**, 308 (2012).
19 L. Sen, L. Diannan and L. Zheng, *Chem. Eng. J*., **211–212**, 46 (2012).
20 V. N. Tien, V. Saravanamuthu, H. N. Huu and K. Jaya, *J. Hazard. Mater*., **182**, 723 (2010).
21 S. K. Maji, Y. H. Kao and C. W. Liu, *Desalination*, **280**, 72 (2011).
22 A. K. Ioannis and I. Z. Anastasios, *Water Res*., **36**, 5141 (2002).
23 D. Pokhrel and T. Viraraghavan, *Chem. Eng. J*., **140**, 165 (2008).
24 V. K. Gupta, V. K. Saini and N. Jain, *J. Colloid Interface Sci*., **288**, 55 (2005).
25 K. Sanghamitra and A. K. Gupta, *J. Hazard. Mater*., **142**, 97 (2007).
26 G. Anjali, Y. Mohammed and S. Nalini, *Ind. Eng. Chem. Res*., **52**, 2066 (2013).
27 R. Ansari and N.K. Fahim, *React. Funct. Polym*., **67**, 367 (2007).
28 R. Ansari and A. Pornahad, *Sep. Sci. Technol*., **45**, 2376 (2010).
29 R. Ansari, B. Seyghali, A. Mohammad-Khah and M. A. Zanjanchi, *Sep. Sci. Technol*., **47**, 1802 (2012).
30 G. Suresh and B. V. Babu, *Bioresour. Technol*., **100**, 5633 (2009).
31 A. Anees, R. Mohd, S. Othman, H. I. Mahamad, Y. C. Yap *et al*., *Desalination*, **247**, 636 (2009).
32 I. D. Mall, V. C. Srivastava, G. V. A. Kumar and I. M. Mishra, *Colloids Surf. A*, **278**, 175 (2006).
33 S. D. Biswas and A. K. Dey, *J. Prakt. Chem*., **21**, 147 (1963).
34 Ö. Ahmet, Ö. Dursun and Ö. Ayla, *Process Biochem*., **39**, 2183 (2004).
35 A. V. Vitela-Rodriguez and J. R. Rangel-Mendez, *J. Environ. Manag*., **114**, 225 (2013).
36 B. Madhumita, M. Arjun, V. V. Srinivasu and S. O. Maurice, *Chem. Eng. J*., **181–182**, 323 (2012).
37 L. Song, S. Zhang, B. Chen, J. Ge and X. Jia, *Colloids Surf., A*, **360**, 1 (2010).

[38] E. O. Augustine and H. Yuh-Shan, *Bioresour. Technol.*, **99**, 5411 (2008).
[39] D. M. Monahar, K. K. Anoop and T. S. Anirudhan, *Water Res.*, **36**, 1609 (2002).
[40] E. J. P. Gérrard, D. Parsonage, B. I. Touma, M. K. Ghosh, E. Paling *et al*., *Int. J. Eng. Sci. Technol.*, **2**, 13 (2010).
[41] I. Langmuir, *J. Am. Chem. Soc*., **40**, 1361 (1918).
[42] U. Freundlich, *Phys. Chem*., **57**, 84 (1906).
[43] R. C. Saidur and K. Y. Ernest, *J. Environ. Manage*., **91**, 2238 (2010).
[44] G. McKay and Y.S. Ho, *Process Biochem*., **34**, 451 (1999).
[45] W. J. J. Weber and J. C. Morriss, *J. Sanitary Eng. Div*., **89**, 31 (1963).
[46] N. R. Khandaker, P. V. Brady and J. L. Krumhans, Arsenic removal from drinking water: A handbook for communities, Sandia National Laboratories Report, 2009.